

STUDY OF THE N_2 $b^1\Pi_u$ STATE VIA 1+1 MULTIPHOTON IONIZATION

Wim UBACHS¹, Lynn TASHIRO and Richard N. ZARE
Department of Chemistry, Stanford University, Stanford, CA 94305, USA

Received 22 June 1988

Medium-resolution spectra of the N_2 $b^1\Pi_u$ - $X^1\Sigma_g^+$ band system were recorded by 1+1 multiphoton ionization. In the spectra we found different linewidths for transitions to different vibrational levels in the $b^1\Pi_u$ state: $\Delta\nu_0 = 0.50 \pm 0.05$ cm^{-1} , $\Delta\nu_1 = 0.28 \pm 0.02$ cm^{-1} , $\Delta\nu_2 = 0.65 \pm 0.06$ cm^{-1} , $\Delta\nu_3 = 3.2 \pm 0.5$ cm^{-1} , $\Delta\nu_4 = 0.60 \pm 0.07$ cm^{-1} , and $\Delta\nu_5 = 0.28 \pm 0.02$ cm^{-1} . From these linewidths, predissociation lifetimes τ_i were obtained: $\tau_0 = 16 \pm 3$ ps, $\tau_1 > 150$ ps, $\tau_2 = 10 \pm 2$ ps, $\tau_3 = 1.6 \pm 0.3$ ps, $\tau_4 = 9 \pm 2$ ps, and $\tau_5 > 150$ ps. Band origins and rotational constants for the $b^1\Pi_u$ $v=0$ and 1 levels were determined for the $^{14}N_2$ and $^{14}N^{15}N$ molecules.

1. Introduction

Much progress is being made on the production of tunable extreme ultraviolet radiation (XUV) in the windowless regime below 105 nm. Two major advances have taken place, the use of synchrotron light sources and the upconversion of coherent light sources in the visible and ultraviolet. Although the former is more broadly tunable, the latter is generally brighter over its more limited tuning range and it can be constructed for far less cost in the laboratory of an individual investigator. In spite of these advances, the spectroscopic application of coherent XUV sources is still in a primitive state because most of these sources have an extremely limited tunability [1]. However, efficient and tunable XUV has been demonstrated in the range 92–102 nm by several investigators [2–4] through third-harmonic generation of the output from a frequency-doubled dye laser.

From their general purpose XUV spectrometer, Softley et al. [3] obtained a 1 XUV+1 UV multiphoton ionization (MPI) spectrum of the $b^1\Pi_u$ $v' = 1 - X^1\Sigma_g^+$ $v'' = 0$ transition in molecular nitrogen. Their resolution, however, did not improve upon the best data for the N_2 $b^1\Pi_u$ state taken with a grating spectrograph [5]. Comparable accuracy in the rota-

tional constants was obtained by Rajan [6] from an analysis of the $b^1\Pi_u$ - $a^1\Pi_g$ emission system. At more moderate resolution the synchrotron radiation absorption spectrum of N_2 in the range 66–100 nm gives an overview of the complex vibronic structure in the N_2 spectrum [7]. Through the extensive high-resolution absorption studies by Carroll and Collins [5] and the deperturbation analysis by Dressler [8], the assignment of the dense vibronic structure in the energy range between 100000 and 106000 cm^{-1} has been clarified. Relative photoabsorption cross sections to different vibrational levels in the $b^1\Pi_u$ valence state and interacting $^1\Pi_u$ Rydberg states have been investigated quantitatively [7,9–11]. A theoretical account of the mutual interferences between b , c and $o^1\Pi_u$ states was given by Stahel et al. [12]. The $X^1\Sigma_g^+$ $v=0$ level has been well characterized through Raman spectroscopy by Bendtsen [13].

In the present paper we present higher-resolution spectra of the N_2 $b^1\Pi_u$ - $X^1\Sigma_g^+$ band system, detected by 1+1 MPI. Because it was known from earlier work [5,8] that severe perturbations occur in the rotational structure of the $b^1\Pi_u$ state vibrational levels with $v > 1$, we analyzed only the $v=0$ and 1 levels in detail. The $b^1\Pi_u$ state has also been observed by 3+1 MPI [14]. For spectroscopic purposes, 1 XUV+1 UV MPI seems preferable to 3+1 MPI because saturation broadening and possible AC-Stark shifting are avoided.

The N_2 $b^1\Pi_u$ state is known to predissociate around

¹ Present address: Natuurkundig Laboratorium, Vrije Universiteit, De Boelelaan 1081, 1081 HV Amsterdam, The Netherlands.

the $v=3$ vibrational level [5,15,16]. From linewidth measurements we estimate predissociation lifetimes for the lower vibrational levels of the $N_2 b^1\Pi_u$ state. The intensity of $(v, 0)$ bands of the $N_2 b^1\Pi_u-X^1\Sigma_g^+$ system varies in the MPI spectrum with v in a manner consistent with the predissociation rates determined from the MPI linewidths.

2. Experimental

The XUV spectrometer is depicted schematically in fig. 1. The vacuum part consists of three differentially pumped chambers. In the tripling chamber the XUV is produced by third harmonic generation of a focused UV laser beam in a pulsed jet of xenon, krypton [2,3] or acetylene [17]. In the sample chamber the N_2 molecules are excited by the diverging XUV/UV beams (beam diameter is 5 mm), emerging from the frequency tripling region. The N_2 was obtained from a pulsed valve (General Valve), with the orifice 25 mm for the interaction region. With a backing pressure of 30 psi we found a rotationally cooled spectrum with $T_{rot}=150$ K. The average pressure in the chamber is maintained below 10^{-5} Torr. The estimated density in the interaction region at the time of the laser pulse is on the order of 10^{-3} Torr, based on a comparison of signal intensities with detection in bulk gas. The nascent ions were extracted through a slit into a time-of-flight (TOF) chamber and mass

selectively detected on a multichannel plate. The mass resolution of the TOF spectrometer is in general 1 in 100, which is sufficient to separate $^{14}N_2$ from $^{14}N^{15}N$. However, the very strong signals at mass 28 ($^{14}N_2$) prevent observation of underlying features of $^{14}N^{15}N$ at mass 29. Strong ion signals at mass 32 caused by $O_2 H^3\Pi_u-X^3\Sigma_g^+$ autoionization transitions in O_2 from O_2 contamination were also observed in different parts of the N_2 spectrum.

The laser system consists of a Quanta-Ray DCR 1A Nd:YAG laser, a PDL1 dye laser and a WEX frequency doubling and tracking device. Special care was taken that the UV power in the range 289.5–298.0 nm was held constant at 9–10 mJ/pulse. Different dye mixtures of rhodamine 590, 610 and 640 (Exciton) were used in several overlapping parts of this wavelength range. For the spectroscopic measurements an air spaced etalon (Moletron) was inserted in the oscillator cavity, resulting in a laser bandwidth in the visible of 0.03 – 0.04 cm^{-1} and a reduction of UV power to 5–8 mJ/pulse. Pressure tuning of the cavity with CO_2 gas allows for continuous scans of 10 cm^{-1} , corresponding to 60 cm^{-1} in the XUV. The residual visible light is used for calibration purposes. The I_2 absorption spectrum and transmission fringes of a calibrated solid etalon (FSR= 0.650 ± 0.001 cm^{-1}) were recorded simultaneously with the MPI spectrum on a three-pen chart recorder. In nonlinear upconversion processes the exact harmonics of the fundamental frequency are produced; therefore, the

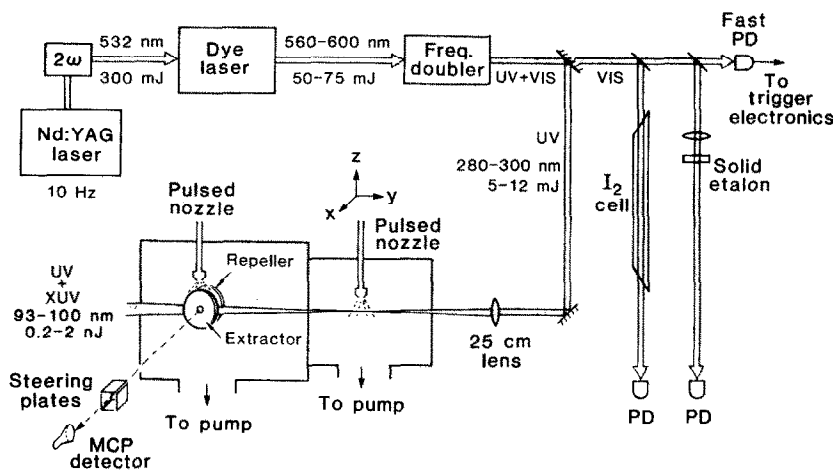


Fig. 1. Schematic diagram of the XUV spectrometer used for 1+1 MPI detection.

accuracy in the observed spectral line positions in the XUV region is directly related to the calibrated I₂ spectrum in the visible.

The XUV power was calibrated in another setup, described in detail by Softley et al. [3]. The XUV is separated from the UV fundamental by a set of two dichroic mirrors and a thin In–Ti foil (Acton Research). The XUV radiation transmitted through the foil is detected on an electron multiplier. The conversion efficiencies for tripling in Xe and Kr fluctuate over more than an order of magnitude within the wavelength range relevant to the experiment. For tripling in acetylene (C₂H₂), the conversion efficiency is substantially less but is nearly wavelength independent between 99.3 and 95.5 nm, i.e. fluctuations are less than 20%. We estimate the number of photons to be 10⁸–10⁹/pulse, corresponding to a power of 0.2–2 nJ/pulse. For the $\nu=3$ linewidth measurements the more efficient krypton and xenon were used as non-linear media. In all cases the power density (in a 5 ns pulse, beam diameter 5 mm) is far too low to saturate a transition at 100 nm. It should be noted that all the MPI studies were performed without the XUV/UV separation unit.

3. Spectroscopy of the N₂ b ¹Π_u $\nu=0$ and $\nu=1$ levels

3.1. ¹⁴N₂

We limited our high-resolution rotational analysis of the b ¹Π_u electronic state to the $\nu=0$ and 1 levels and did not attempt to analyze the higher ν levels because they are known to be perturbed. A medium resolution spectrum of the (1, 0) bandhead portion of the ¹⁴N₂ b ¹Π_u–X ¹Σ_g⁺ system is shown in fig. 2. The exact position of the spectral lines was determined from interpolation between I₂ lines that are accurately tabulated [18,19]. Single resolved rotational lines have an experimental linewidth of 0.3 cm⁻¹ in the XUV. We therefore estimate an error of ±0.03 cm⁻¹ in the absolute position of the strong N₂ lines and ±0.06 cm⁻¹ for the weaker ones, i.e. those for $J>18$ in the (1, 0) band and the lines in the (0, 0) band. Tables 1 and 2 list the line positions of all observed N₂ b ¹Π_u–X ¹Σ_g⁺ (0, 0) and (1, 0) transitions, respectively. The data were fit in a least-squares manner to Hamiltonians of the form

$$H = B_v[J(J+1) - A^2] - D_v[J(J+1) - A^2]^2, \quad (1)$$

for both the b ¹Π_u and X ¹Σ_g⁺ states. In the fit of the (0, 0) band we included the line positions for transitions to higher J states from Carroll and Collins [5]. The rotational constant B and the centrifugal distortion constant D for the $\nu=0$ level of the ground state were fixed at the very accurate values of Bendtsen [13], obtained by rotational Raman spectroscopy: $B_0 = 1.98574(12)$ cm⁻¹ and $D_0 = 5.76(3) \times 10^{-6}$ cm⁻¹. The resulting B and D constants for the b ¹Π_u $\nu=0$ and $\nu=1$ levels, listed in table 3, are an order of magnitude more accurate than the best known values [5,6]. For all the data the experimental and calculated values match within twice the estimated errors. Therefore, we conclude that the rotational structure of the N₂ b ¹Π_u, $\nu=0$ and $\nu=1$ levels is well behaved. An attempt to include a A -doubling constant for either the b ¹Π $\nu=0$ or $\nu=1$ level in the least-squares fit yielded no significant improvement. Based on a two-standard-deviation error, we conclude that $q < 4 \times 10^{-4}$ cm⁻¹ for the $\nu=0$ level and $q < 5 \times 10^{-5}$ cm⁻¹ for the $\nu=1$ level.

3.2. ¹⁴N ¹⁵N

The mass selectivity and the high sensitivity of our XUV spectrometer allowed us to measure the spectrum of the b ¹Π_u–X ¹Σ_g⁺ transition of the ¹⁴N¹⁵N molecule in natural abundance (0.74%). It is the first observation of the b–X system for the ¹⁴N¹⁵N molecule. Fig. 3 shows a recording of the bandhead portion of the b ¹Π_u–X ¹Σ_g⁺ (0, 0) transition for ¹⁴N₂ and ¹⁴N¹⁵N. It should be noted that the apparent sensitivity difference of a factor of 48 does not reflect the natural abundance ratio between the two isotopes. It is known that heavier isotopes are often less predissociated [20]. Robbe [16] found that for the b ¹Π_u–X ¹Σ_g⁺ (3, 0) transition ¹⁵N₂ was a factor of 2.7 less predissociated than ¹⁴N₂. We estimate that ¹⁴N¹⁵N is a factor of 2.8 less predissociated than ¹⁴N₂ for the b ¹Π_u–X ¹Σ_g⁺ (0, 0) transition. The observed line positions are presented in table 4 for the (0, 0) band and in table 5 for the (1, 0) band. As mentioned previously, the ¹⁴N¹⁵N rotational lines that coincide with very strong ¹⁴N₂ lines could not be separated in the mass selective ion detector. For the weak (0, 0) band, only the rotational lines in the 12 cm⁻¹

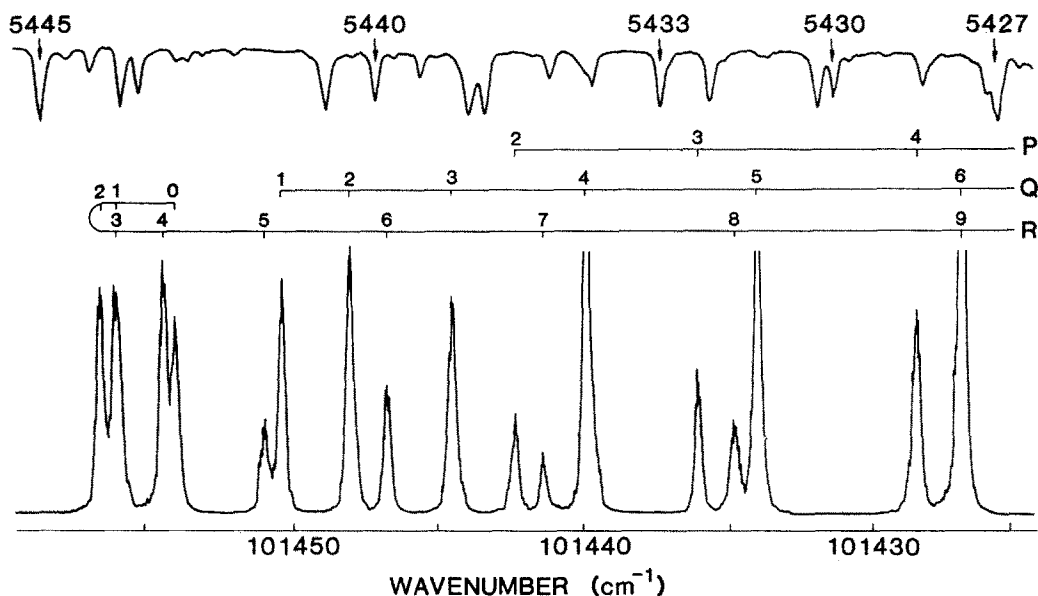


Fig. 2. Bandhead portion of the 1 XUV+1 UV MPI spectrum of $N_2 b^1\Pi_u-X^1\Sigma_g^+$ (1,0) band. The upper curve shows the simultaneously recorded I_2 absorption spectrum. The numbering of the I_2 lines refers to the I_2 atlas [18,19].

region at the high energy side of the $^{14}N_2$ (0,0) band-head were observed.

Band origins and rotational constants for the $b^1\Pi_u$, $v=0$ and $v=1$ levels, obtained from a least-squares

fit, are listed in table 3. Again, the ground state constants were fixed on the values from Raman spectroscopic data [13]: $B_0 = 1.923596(9) \text{ cm}^{-1}$ and $D_0 = 5.38(3) \times 10^{-6} \text{ cm}^{-1}$. Because we measured only

Table 1

Line positions (in cm^{-1}) for the $^{14}N_2 b^1\Pi_u-X^1\Sigma_g^+$ (0,0) band. The estimated uncertainty in the line positions is $\pm 0.06 \text{ cm}^{-1}$, while the lines with b are blended (uncertainty is $\pm 0.15 \text{ cm}^{-1}$)

J	R(J)		Q(J)		P(J)	
	observed	obs. - calc	observed	obs. - calc	observed	obs. - calc.
0	100819.70	-0.01				
1	100821.51	-0.01	100815.75	0.02		
2	100822.31	0.07	100813.68	0.11	100807.69	-0.08
3	100821.93	0.05	100810.47	0.16	100801.56	-0.06
4	100820.46	0.04	100805.88	-0.08	100794.30	-0.09
5	100817.95	0.07	100800.47	-0.06	100786.10	0.03
6	100814.21	-0.02	100794.05	0.04	100776.57	-0.09
7	100809.61	0.12	100786.30	-0.09	100766.19	-0.03
8	100803.69	-0.05	100777.70	0.03	100754.52	0.04
9	100796.69	0.01	100767.86	0.01	100741.84	-0.03
10	100788.95	-0.03	100756.70	-0.21b	100728.15	0.07
11	100779.40	0.05	100744.55	-0.32b	100713.32	0.14
12			100731.74	0.03b	100697.26	0.06
13			100717.46	-0.03	100697.26	0.06
14			100702.11	0.11		
15			100685.58	0.14		

Table 2

Line positions (in cm^{-1}) for the $^{14}\text{N}_2$ b $^1\Pi_u$ -X $^1\Sigma_g^+$ (1, 0) band. The estimated uncertainty in the line positions is $\pm 0.03 \text{ cm}^{-1}$ for the lower J and $\pm 0.06 \text{ cm}^{-1}$ for $J > 18$, while the lines with b are blended (uncertainty is $\pm 0.15 \text{ cm}^{-1}$)

J	R(J)		Q(J)		P(J)	
	observed	obs. – calc.	observed	obs. – calc.	observed	obs. – calc.
0	101454.485	0.015				
1	101456.055	-0.067	101450.471	-0.020		
2	101457.602	-0.008	101448.153	-0.011	101442.527	-0.006
3	101456.055	0.123	101444.666	-0.007	101436.239	0.011
4	101454.104	0.016	101440.051	0.034	101428.750	-0.008
5	101451.035	-0.041	101434.191	-0.004	101420.148	0.024
6	101446.864	-0.030	101427.19	-0.01b	101410.318	-0.007
7	101441.553	0.011	101419.049	0.001	101399.26	-0.10b
8	101434.978	-0.038	101409.724	0.004	101387.41	0.19b
9	101427.19	-0.12b	101399.26	0.04b	101373.953	0.028
10	101418.484	0.048	101387.41	-0.13b	101359.466	0.014
11	101408.376	0.001	101374.707	0.012	101343.843	0.037
12	101397.127	-0.003	101360.637	-0.028	101327.000	0.015
13	101384.711	0.012	101345.436	-0.016	101308.970	-0.016
14	101371.077	0.002	101329.051	-0.003	101289.773	-0.034
15	101356.260	-0.001	101311.440	-0.027	101269.458	0.013
16	101340.258	0.013	101292.689	0.009	101247.862	-0.033
17	101323.031	0.004	101272.672	-0.041	101225.196	0.040
18	101304.587	-0.015	101251.630	0.093	101201.278	0.056
19	101284.986	0.021	101229.227	0.071	101176.133	0.042
20	101264.141	0.030	101205.594	0.027	101149.792	0.034
21	101242.035	-0.004	101180.783	0.020	101122.197	-0.021
22	101218.775	0.042	101154.805	0.065	101093.490	0.023
23	101194.099	-0.096	101127.420	-0.071	101063.454	-0.045
24	101168.464	0.044	101099.028	0.014	101032.264	-0.047
25	101141.368	-0.030	101069.359	0.058	100999.867	-0.029
26	101113.108	-0.017	101038.370	0.024	100966.237	-0.011
27			101006.118	-0.024		
28			100972.712	0.028		

Table 3

Spectroscopic constants (in cm^{-1}) for the b $^1\Pi_u$ $\nu=0$ and 1 states of $^{14}\text{N}_2$ and $^{14}\text{N}^{15}\text{N}$. The cited uncertainties represent two standard deviations

	$\nu=0$		$\nu=1$	
$^{14}\text{N}_2$	B_0	1.4478 ± 0.0003	B_1	1.4078 ± 0.0001
	$10^5 D_0$	2.82 ± 0.04	$10^5 D_1$	1.581 ± 0.015
	ν_{00}	100818.263 ± 0.033	ν_{10}	101453.063 ± 0.011
$^{14}\text{N}^{15}\text{N}$	B_0	1.4017 ± 0.0056	B_1	1.3619 ± 0.0004
	$10^5 D_0$	$2.64 \pm 0.04^{\text{a)}}$	$10^5 D_1$	1.50 ± 0.07
	ν_{00}	100831.60 ± 0.18	ν_{10}	101455.016 ± 0.033

^{a)} $D_0(^{14}\text{N}^{15}\text{N})$ was frozen at 2.64×10^{-5} in the fit and calculated from the D_0 value for $^{14}\text{N}_2$ and the isotope relation, $D_0(^{14}\text{N}^{15}\text{N}) = \rho^4 D_0(^{14}\text{N}_2)$.

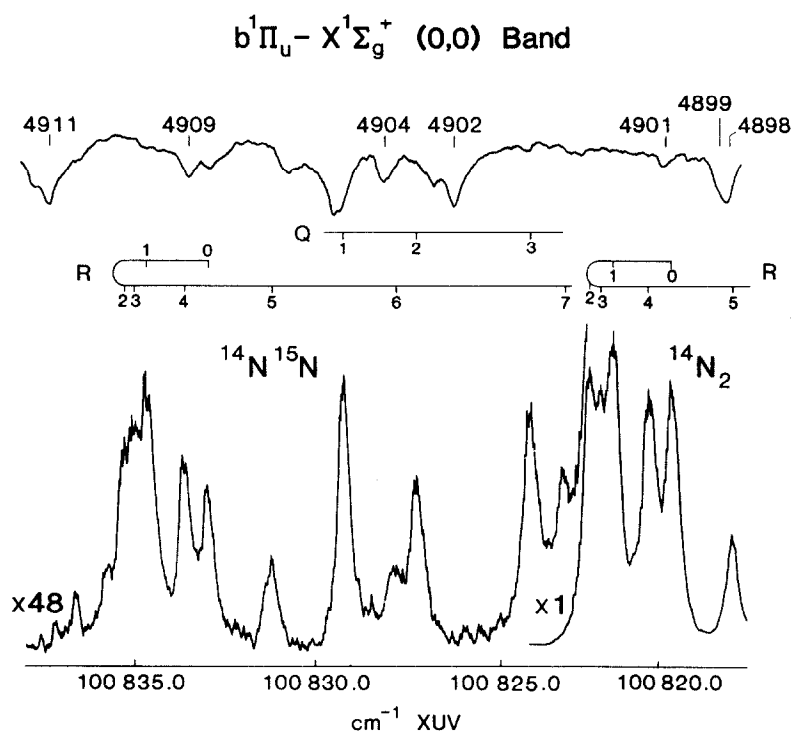


Fig. 3. Bandhead portion of the 1 XUV + 1 UV MPI spectra of $N_2 b^1\Pi_u - X^1\Sigma_g^+ (0,0)$ transition for $^{14}N_2$ and $^{14}N^{15}N$. The upper curve shows the simultaneously recorded I_2 absorption spectrum.

transitions to low J states in the $(0,0)$ band, we did not obtain a value for the centrifugal distortion constant. Experimentally derived values have been compared to those predicted by the isotopic relations

Table 4

Line positions (in cm^{-1}) for the $^{14}N^{15}N b^1\Pi_u - X^1\Sigma_g^+ (0,0)$ band. The estimated uncertainty in the line positions is $\pm 0.15 cm^{-1}$. Lines with b are blended

J	R(J)		Q(J)	
	observed	obs. - calc.	observed	obs. - calc.
0	100832.84	-0.16		
1	100834.62	-0.14b	100829.39	0.24
2	100835.36	-0.11b	100827.27	0.21
3	100835.01	-0.13b	100824.20	0.27
4	100833.39	-0.36		
5	100831.37	0.05		
6	100827.91	0.08		
7	100823.34	0.06		

$B_v(^{14}N^{15}N) = \rho^2 B_v(^{14}N_2)$ and $D_v(^{14}N^{15}N) = \rho^4 D_v(^{14}N_2)$, with $\rho = 0.983349$ [21]. Although these Dunham relations hold only rigorously for the equilibrium constants [22], they yield a good approximation for the lowest vibrational levels $v=0$ and 1. The derived B_1 and D_1 constants for the $b^1\Pi_u v=1$ level of $^{14}N_2$ and $^{14}N^{15}N$ obey the isotopic substitution rules within the error limits. The same is true for the B_0 constant of the $v=0$ level. This suggests that there is a negligible coupling between electronic and rotational motion in the molecule. On the other hand, the anomalously large value for the centrifugal distortion for $v=0$ ($^{14}N_2$) argues against this.

4. Predissociation

4.1. Linewidth measurements

Absolute values for the lifetimes of excited states can be derived from measurements of the line broad-

Table 5

Line positions (in cm^{-1}) for the $^{14}\text{N}^{15}\text{N } b^1\Pi_u - X^1\Sigma_g^+$ (1, 0) band. The estimated uncertainty in the line positions is $\pm 0.04 \text{ cm}^{-1}$. Lines with b are blended (uncertainty is $\pm 0.15 \text{ cm}^{-1}$)

J	R(J)		Q(J)		P(J)	
	observed	obs. – calc.	observed	obs. – calc.	observed	obs. – calc.
1	101457.872	–0.10b	101450.471	–0.026		
2	101458.403	0.050				
3	101457.872	0.07b			101438.756	0.013
4					101431.560	0.034
5	101453.145	0.020	101436.788	–0.007	101423.011	0.173
6	101449.045	–0.047	101430.080	0.034	101413.741	0.024
7	101443.918	–0.011	101422.052	–0.117	101403.101	–0.02b
8	101437.620	–0.013	101413.178	0.015	101391.560	0.155
9			101403.101	0.077	101378.573	0.018
10	101421.519	–0.112	101391.900	0.148	101364.608	0.033
11	101411.898	–0.027	101379.377	0.034	101349.468	0.006
12	101401.132	0.058	101365.805	0.009		
13			101357.127	0.019	101315.799	–0.031
14					101297.338	0.032
15			101318.299	0.005	101277.617	–0.022
16			101300.146	–0.015	101256.816	–0.010
17			101280.834	–0.040	101234.841	–0.024
18			101260.481	0.052	101211.705	–0.045
19			101238.852	0.032		
20			101216.014	–0.029		
21			101192.056	–0.039		
22			101166.985	0.015		
23			101140.688	0.025		

ening. Fig. 4 shows spectra of one or more well resolved rotational lines of transitions from $X^1\Sigma_g^+$ $v''=0$ to the $b^1\Pi_u$ $v'=0$ to $v'=5$ levels. The line-widths were recorded relative to the distance ($3.90 \pm 0.06 \text{ cm}^{-1}$ in the XUV) between interference fringes of a solid etalon. The lines in the (3, 0) band are very broad and weak. The rotational structure of the band is such that there are almost no unblended lines. The bandhead is very congested and the R(19) line is one of the few well resolved lines. Fig. 5 shows a recording of the bandhead portion of the $b^1\Pi_u$ (3, 0) band. In contrast to all other line-width measurements, this spectrum was taken using acetylene as the tripling medium without an intracavity etalon in the dye laser at an instrumental width of 1.2 cm^{-1} . Line position assignments for the $b^1\Pi_u$ (3, 0) band were obtained using the results and procedure of Carroll and Collins [5]. The differences between calculated deperturbed and observed energy levels were plotted versus $J(J+1)$. A curve through

these points yielded the assignments of Carroll and Collins for the high J transitions. The curve was extrapolated to give assignments to transitions not measured by Carroll and Collins including the congested bandhead. For the other bands only a few rotational lines in the P, Q and R branches were overlapped. The widths of several observed lines were averaged, and the results are listed in table 6. The linewidth of transitions to the $v'=1$ and $v'=5$ levels and also the $v'=6$ and $v'=7$ levels, not shown here, is 0.28 cm^{-1} . These levels are not predissociated and the value of 0.28 cm^{-1} represents the combined effect of the sextupled dye laser bandwidth and Doppler broadening. The additional broadening for the other $b^1\Pi_u$ v levels is caused by the fast predissociation rate. The width and the lifetime are related through the uncertainty principle:

$$\tau = (2\pi\Gamma c)^{-1}, \quad (2)$$

where Γ is the intrinsic linewidth in cm^{-1} related to

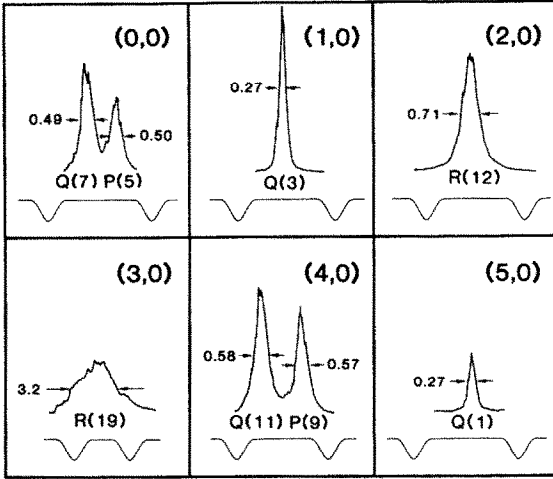


Fig. 4. Linewidths (in cm^{-1}) for single rotationally resolved lines for the $N_2 b^1\Pi_u-X^1\Sigma_g^+$ ($v, 0$) bands for $v=0$ to 5. The interference fringes (lower trace) represent a frequency distance of 3.90 cm^{-1} in the XUV.

the lifetime τ of the state and c is the speed of light in cm/s . The frequency profile of the observed transitions to $v=1$ and $v=5$ appears to be Gaussian. A homogeneous line broadening effect, producing a Lorentzian width Γ , can be deconvoluted from an observed width $\Delta\nu_{\text{obs}}$ in cm^{-1} by [23]:

$$\Gamma = \Delta\nu_{\text{obs}} - (\Delta\nu_{\text{instr}})^2 / \Delta\nu_{\text{obs}}, \quad (3)$$

when the instrumental profile is Gaussian. In eq. (3) all the widths are taken at full width at half maximum (fwhm). Using eqs. (2) and (3), lifetimes for the $b^1\Pi_u v$ levels were calculated. Results are given in table 6.

In any multiphoton process, competition between radiative and predissociation effects and the driving force of ionization will affect the field free natural lifetime of an excited state. Shortening of the lifetime because of a depletion of the excited state population by the ionization step can be neglected in the present 1+1 MPI detection scheme with diverging laser beams, at least for the rapidly predissociated levels. The $v=1$ and 5 states, with radiative lifetimes in the nanosecond regime will indeed be somewhat lifetime shortened under the conditions of the present experiment but not on a scale detectable as lifetime broadening. Also a broadening effect caused by saturation of the first photon step $b^1\Pi_u-X^1\Sigma_g^+$ can be ruled out

in view of the XUV power density. Therefore, we conclude that the lifetimes, as listed in table 6, represent the natural lifetimes of the $N_2 b^1\Pi_u$ states.

The line broadening measurements give direct evidence for predissociation in the vibrational levels $v=0, 2, 3$ and 4 and reasonably accurate values for a nonradiative lifetime, as listed in table 4. The unbroadened $b^1\Pi_u v=1, 5$ and 6 levels coincide with the ones that are also observed in $b^1\Pi_u-a^1\Pi_g$ ultraviolet emission [6,24–26] or in $b^1\Pi_u-X^1\Sigma_g^+$ vacuum ultraviolet emission [27].

4.2. Intensity measurements

An overview spectrum of the $N_2 b^1\Pi_u-X^1\Sigma_g^+$ system is presented in fig. 6. It shows the vibrational sequence in the $b^1\Pi_u$ state from $v=0$ to $v=4$. In order to tune the laser easily over the wide wavelength range from 573 to 596 nm (95.5 to 99.3 in the XUV) the etalon was not used. The spectrum was taken in overlapping parts, but over the whole range the XUV as well as the UV power were kept constant. This was established by using different dye mixtures and by tripling in C_2H_2 . We estimate that the XUV power is less than 10^9 photons/pulse, the bandwidth in the XUV is $\approx 1.0 \text{ cm}^{-1}$, and the UV power is 10 mJ/pulse. In table 7 the estimated peak intensities for the 1+1 MPI spectra of the $N_2 b^1\Pi_u-X^1\Sigma_g^+$ transitions are listed. Because the data collection has not been computerized, no attempt was made to obtain integrated band intensities or even integrated line intensities.

The line intensities in our 1+1 MPI spectra do not agree with either calculated or observed absorption intensities. In table 7 the MPI intensities are compared with values for photoabsorption cross sections and intensities [5,7,10,11] from electron energy loss spectroscopy (EELS) [28]. Stahel et al. [12] calculated relative absorption intensities in a treatment where the interference between the $b^1\Pi_u$ valence state and two Rydberg states of the same symmetry, denoted by $c^1\Pi_u$ and $o^1\Pi_u$, were included. Only the two ratios of the deperturbed electronic transition moments, $(b-X)/(c-X)$ and $(b-X)/(o-X)$, were fitted to the EELS data; the vibrational intensity distribution, including the detailed vibronic intensity interferences, was found from the energy deperturbation without additional fitting to the observed in-

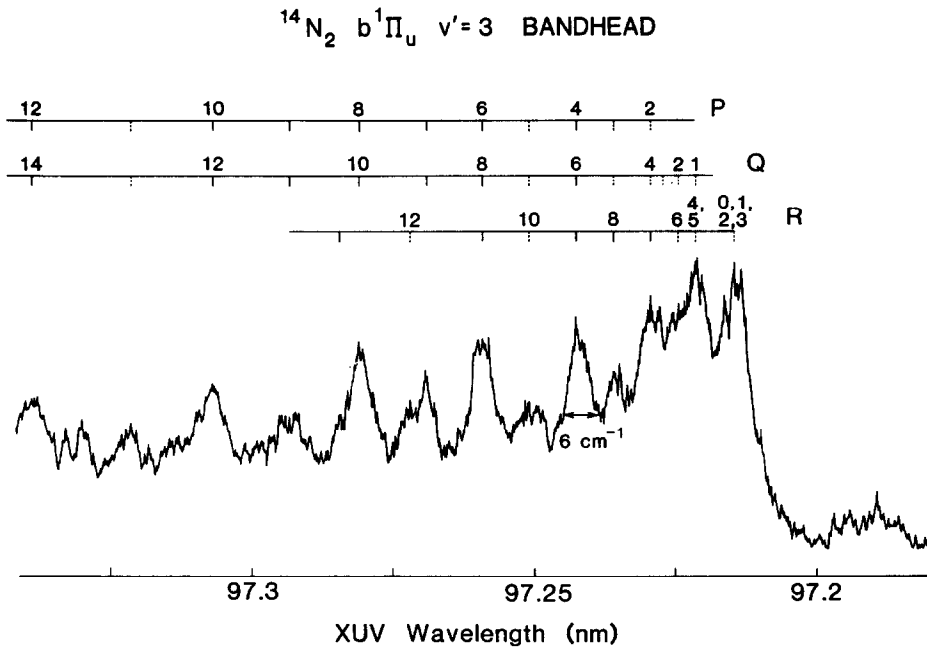


Fig. 5. Bandhead portion of the 1 XUV + 1 UV MPI spectrum of $N_2 b^1\Pi_u - X^1\Sigma_g^+ (3,0)$ band. Solid lines denote transitions observed by Carroll and Collins [5] and broken lines denote transitions assigned by the extrapolation procedure. Acetylene was used as the tripling medium and the dye laser was operated without the intracavity etalon providing an instrumental linewidth of 1.2 cm^{-1} .

tensity distribution. The calculations are in agreement with the global features of observed intensities of photoabsorption cross sections, not only for the lowest vibrational levels as discussed here but also for the higher levels up to $v=15$, including the sharp intensity falloffs at $v=5$ and 8. This indicates that the one-photon excitation of the $b^1\Pi_u$ state is well understood.

When compared with absorption data, the $b^1\Pi_u$ $v=1, 5, 6$ and 7 levels appear relatively strong in the

Table 6
Observed linewidths and calculated lifetimes for the $^{14}N_2 b^1\Pi_u v$ levels

v level	$\Delta\nu_{\text{obs}} (\text{cm}^{-1})$	$\tau_v (\text{ps})$
0	0.50 ± 0.05	16 ± 3
1	0.28 ± 0.02	> 150
2	0.65 ± 0.06	10 ± 2
3	3.2 ± 0.5	1.6 ± 0.3
4	0.60 ± 0.07	11 ± 2
5	0.28 ± 0.02	> 150

MPI spectra; this is the behavior expected for unpre-dissociated levels. The observed 1+1 MPI spectral intensities (see fig. 6) are a factor 8 ($v=0$), 13 ($v=2$), 230 ($v=3$), and 40 ($v=4$) weaker relative to the $v=1$ level when the calculated absorption strengths [12] are accounted for (see table 7). These factors indicate again, at least qualitatively, that the $v=3$ level is very strongly predissociated, while the $v=2$ and 4 levels show less predissociation. The line intensity loss on the $v=4$ level is more than the loss on the $v=2$ level, while the predissociation rates are the same within experimental error. At the same time, however, Stahel et al. [12] used a value for the relative absorption cross section for $v=4$ in their analysis based on the work of Geiger and Schroeder [28]. This value is higher than the more recent synchrotron value of Grtler et al. [7], but the synchrotron data appear to be taken at such a high number density (see Lawrence, Mickey and Dressler [10]) that the absolute oscillator strengths are affected by line saturation. Although the lower value for $\sigma_{\text{abs}}(v=4)$ from the synchrotron data would bring the present MPI inten-

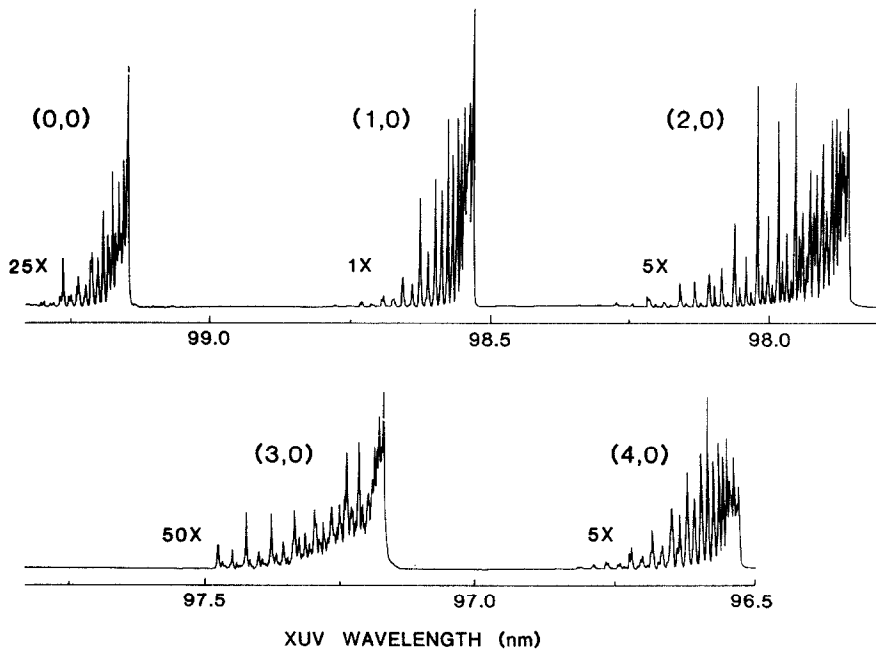


Fig. 6. Overview spectrum of the $N_2 b^1\Pi_u - X^1\Sigma_g^+$ system covering the $(\nu, 0)$ bands for $\nu=0$ to 4. The numbers next to the different bands represent a multiplication factor for the sensitivity of the detector.

sities in agreement with the lifetimes and predissociation rates, the use of these data does not appear to be justified. The $\nu=0$ level has the longest lifetime of

the predissociated levels discussed here. The smallest change in intensity for this level is consistent with this fact.

Table 7

Cross sections for different $^{14}N_2 b^1\Pi_u - X^1\Sigma_g^+$ vibronic transitions. The photoabsorption data are given as absolute cross sections (in Mb), while the data in the last three columns represent relative cross sections

ν	Photoabsorption				EELS ^{e)}	Calc. ^{f)}	1+1 MPI ^{g)}
	a)	b)	c)	d)			
0				18	28	34	3
1	57			16	160	153	100
2	253	75		80	350	385	20
3	357	124	200	300	640	712	2
4	321	125	550	100	1000	972	15
5	44	30		16	50	40	15

^{a)} Gürtler et al. [7]; absorption of synchrotron radiation.

^{b)} Carter [9]; absorption of a helium lamp continuum, derived from fig. 3 of this reference.

^{c)} Lawrence et al. [10]; calculated from oscillator strength, thereby setting $f=0.055$ equal to 550 Mb.

^{d)} Huffman et al. [11]; absorption of a helium lamp continuum. The cross sections in Mb were calculated from absorption strengths k in cm^{-1} .

^{e)} Geiger and Schroeder [28]; electron energy loss of 25 keV electrons.

^{f)} Stahel et al. [12]; calculations, fitted and normalized to data under e).

^{g)} This work.

The 1+1 MPI signal intensity for the $v=5$ level is a factor of 7 lower than for the $v=1$ level. In the EELS data [28] and in the calculation [12] the intensity reduction for $v=5$ relative to $v=1$ is only a factor 3–4, whereas in the photoabsorption measurements [7,11] both bands appear equally strong. The relatively low intensity on the $v=5$ level might be explained by a slow rate of predissociation not detectable by line broadening.

5. Discussion

The N_2 b $^1\Pi_u$ state is a celebrated example of predissociation in diatomic molecules [20]. The first quantitative analysis of predissociation rates as a function of vibrational level was performed by Leoni and Dressler [15] for the N_2 b–X band system. The N_2 b $^1\Pi_u$ state lies above the $N(^4S)+N(^4S)$ and $N(^4S)+N(^2D)$ dissociation limits and is extensively predissociated. Using photoelectric recording and fitting the band profiles as a function of pressure, Leoni and Dressler deduced the widths for the $v=0, 1, 2, 3,$ and 4 levels: $\Gamma_0=0.13$ cm $^{-1}$, $\Gamma_1<0.003$ cm $^{-1}$, $\Gamma_2=0.20$ cm $^{-1}$, $\Gamma_3=20.0$ cm $^{-1}$, and $\Gamma_4=0.25$ cm $^{-1}$ where Γ represents the width caused by predissociation. Leoni and Dressler suggested that an interaction between the b $^1\Pi_u$ state and the continuum of the $C' ^3\Pi_u$ state was responsible for the predissociation of the b $^1\Pi_u$ state. This direct (spin–orbit) predissociation mechanism is able to predict that the $v=0$ and 2 levels are broadened by the amount observed, while the $v=1$ level remains sharp. However, this model cannot account for the unusually large width of the $v=3$ level and the more modest width of the $v=4$ level. Leoni and Dressler suggested that the b $^1\Pi_u$ $v=3$ level interacts with a nearby diffuse level identified as the $F ^3\Pi_u$ $v=0$ level, based on the observation by Ogawa and Tanaka [29] of higher members of this triplet Rydberg series. The diffuseness of the levels of the $F ^3\Pi_u$ state is postulated to arise from an interaction with the continuum of the $C' ^3\Pi_u$ state. Leoni and Dressler speculate that this coupling may also contribute to the observed widths of the b $^1\Pi_u$ $v=2$ and $v=4$ levels.

The triplet states of N_2 have been studied by Joyez et al. [30] using electron impact. Two types of experiments were performed: (1) electron energy loss

measurements for various scattering angles at a fixed incident energy (14.3 eV); and (2) threshold energy electron measurements in which nearly zero kinetic energy electrons are recorded as a function of the incident electron energy for the range 11.8–13.8 eV as well as scattering angle. In the energy loss spectra the dominant features, which showed no angular dependence, correspond to vibrational excitation of the b $^1\Pi_u$ state. In threshold excitation spectra the b $^1\Pi_u$ state is only weakly excited and the spectrum is dominated by features assigned to various vibrational levels of different triplet states. Joyez et al. were able to identify three vibrational levels of a singlet–triplet system on the basis of angular dependence of the intensity whose upper levels were assigned to $v=1, 2,$ and 3 of the $F ^3\Pi_u$ state. This assignment would make the $v=0$ level of the $F ^3\Pi_u$ state coincide with the b $^1\Pi_u$ $v=3$ level, in support of Leoni and Dressler's interpretation. However, the angular dependence of the peak at b $^1\Pi_u$ $v=3$ did not indicate an appreciable triplet contribution.

More recently, Hammond et al. [31] have recorded the threshold electron energy spectrum of N_2 at higher resolution. Their measurements support the suggestion of Joyez et al. [30] that the $F ^3\Pi_u$ state is excited at threshold. Hammond et al. conclude that the b $^1\Pi_u$ $v=3$ feature in their threshold energy spectrum may be a sum of the direct excitation of the b $^1\Pi_u$ $v=3$ and $F ^3\Pi_u$ $v=0$ levels and a resonance decay to either or both of these states.

Robbe [16] reinvestigated the predissociation of the b $^1\Pi_u$ $v=3$ level using photographic techniques. He found a significantly smaller width for the $v=3$ level than Leoni and Dressler, namely, $\Delta\nu_3=3$ cm $^{-1}$ for $^{14}N_2$ and $\Delta\nu_3=1.5$ cm $^{-1}$ for $^{15}N_2$, corresponding to $\Gamma_3=2.7$ cm $^{-1}$ for $^{14}N_2$ and $\Gamma_3=1$ cm $^{-1}$ for $^{15}N_2$. Robbe proposed an alternative explanation for the large width of the b $^1\Pi_u$ $v=3$ level. The b $^1\Pi_u$ $v=3$ level interacts strongly by spin–orbit coupling with the quasi-degenerate $C ^3\Pi_u$ $v=8$ level which, in turn, is predissociated by the continuum levels of the $C' ^3\Pi_u$ state. This interpretation is the one favored by Lefebvre-Brion and Field [20]. Both spectroscopic and predissociation phenomena in the $C ^3\Pi_u$ and $C' ^3\Pi_u$ states have been studied by Carroll and Mulliken [32] and by Ledbetter and Dressler [33]. From a calculation of spin–orbit matrix elements between the $C ^3\Pi_u$ and b $^1\Pi_u$ states, Robbe derived a width

$\Gamma_{3,\text{calc}} = 1.7 \text{ cm}^{-1}$, somewhat smaller than the experimental value. However, the calculated line broadening for vibrational levels other than $v=3$ on the basis of these matrix elements is much smaller than observed. Consequently, an interaction with the $C^3\Pi_u$ state cannot account for all the predissociation effects.

Robbe argues against the hypothesis that the $F^3\Pi_u$ $v=0$ level is the main perturber of the $b^1\Pi_u$ $v=3$ level. Actually, Robbe [16] prefers to renumber the vibrational levels of the $F^3\Pi_u$ state so that the level assigned by Joyez et al. [30] and by Hammond et al. [31] to $v=1$ is instead $v=0$. Even if the $F^3\Pi_u$ $v=0$ level is coincident with the $b^1\Pi_u$ $v=3$ level, Robbe believes that these two levels are not coupled by spin-orbit interaction because the electronic configurations of the F and b states differ by two molecular orbitals. In contrast, the configurations of the C and b states are the same in the energy region considered. Although the $v=8$ level of the state has not been directly observed, Hammond et al. have identified in the energy region near 11 eV the first four vibrational levels of this state, but the intensity in their threshold energy spectrum decreased rapidly with increasing v .

In the present study, we have determined accurate linewidths for the $v=0, 2, 3$ and 4 levels of the $^{14}N_2$ $b^1\Pi_u$ state from which we have derived the following predissociation widths: $\Gamma_0 = 0.34 \pm 0.05 \text{ cm}^{-1}$, $\Gamma_2 = 0.53 \pm 0.05 \text{ cm}^{-1}$, $\Gamma_3 = 3.2 \pm 0.5 \text{ cm}^{-1}$, and $\Gamma_4 = 0.47 \pm 0.05 \text{ cm}^{-1}$. Comparison with the previous work of Leoni and Dressler shows that their widths are a factor of 2.5 smaller except for $v=3$, which is excessively large. Leoni and Dressler determined natural linewidths from a curve of growth analysis by measuring apparent absorption at different pressures. They did not directly measure the linewidths because their experimental apparatus provided an instrumental width of only 4 cm^{-1} . In contrast, our linewidths were directly measured from our spectra. Our measurement of Γ_3 agrees within experimental error with that of Robbe. Leoni and Dressler suggest that their 20.0 cm^{-1} width applies to the low J levels of the $b^1\Pi_u$ $v=3$ level. However, we have examined the $(3,0)$ bandhead which is formed at low J and found closely spaced structure (see fig. 5). Because of the congestion at the bandhead, we cannot determine a linewidth, but we estimate an upper limit for the linewidth of the lower J levels to be Γ_3 (low J) $< 5.8 \text{ cm}^{-1}$.

The dispute between the interpretations of Leoni and Dressler [15] and that of Robbe [16] concerns whether the $b^1\Pi_u$ $v=3$ level interacts with the dissociative $C^3\Pi_u$ state via the $F^3\Pi_u$ $v=0$ level or the $C^3\Pi_u$ $v=8$ level. Unfortunately, the electron impact data of Joyez et al. [30] and Hammond et al. [31] cannot resolve this question unambiguously, and the possibility of both interactions contributing has not been ruled out. Our own measurements also do not settle this question, although they contribute to a better understanding of the predissociation rate. It may be that the observed accidental predissociation of the $b^1\Pi_u$ state is more complicated than previously suspected.

Acknowledgement

We thank R.W. Field for making available to us the thesis of J.M. Robbe and gratefully acknowledge the valuable comments from K. Dressler and H. Lefebvre-Brion. We would also like to acknowledge the National Science Foundation under NSF PHY 85-06668 for its support of this research.

References

- [1] J.F. Reintjes, *Nonlinear optical parametric processes in liquids and gases* (Academic Press, New York, 1984).
- [2] E.E. Marinero, C.T. Rettner, R.N. Zare and A.H. Kung, *J. Phys. Chem.* 88 (1983) 486.
- [3] T.P. Softley, W.E. Ernst, L.M. Tashiro and R.N. Zare, *Chem. Phys.* 116 (1987) 299.
- [4] R.H. Page, R.J. Larkin, A.H. Kung, Y.R. Shen and Y.T. Lee, *Rev. Sci. Instr.* 58 (1987) 1616.
- [5] P.K. Carroll and C.P. Collins, *Can. J. Phys.* 47 (1969) 563.
- [6] K.J. Rajan, *Proc. Roy. Irish Acad.* 74A (1974) 17.
- [7] P. Gurtler, V. Saile and E.E. Koch, *Chem. Phys. Letters* 48 (1977) 245.
- [8] K. Dressler, *Can. J. Phys.* 47 (1969) 547.
- [9] V. Carter, *J. Chem. Phys.* 56 (1972) 4195.
- [10] G.M. Lawrence, D.L. Mickey and K. Dressler, *J. Chem. Phys.* 48 (1968) 1989.
- [11] R. Huffman, Y. Tanaka and J.C. Larrabee, *J. Chem. Phys.* 39 (1963) 910.
- [12] P. Stahel, M. Leoni and K. Dressler, *J. Chem. Phys.* 79 (1983) 2541.
- [13] J. Bendtsen, *J. Ram. Spectry.* 2 (1974) 133.
- [14] S.T. Pratt, P.M. Dehmer and J.L. Dehmer, *J. Chem. Phys.* 81 (1984) 3444.

- [15] M. Leoni and K. Dressler, *J. Appl. Math. Phys. (ZAMP)* 22 (1971) 794.
- [16] J.M. Robbe, Ph.D. Thesis, Université des Sciences et Techniques de Lille, 1978, Lille, France.
- [17] L. Tashiro, W. Ubachs and R.N. Zare, unpublished results.
- [18] S. Gerstenkorn and P. Luc, *Atlas du spectroscopie de la molécule d'iode (CNRS, Paris, 1978)*.
- [19] S. Gerstenkorn and P. Luc, *Rev. Phys. Appl.* 14 (1979) 791.
- [20] H. Lefebvre-Brion and R.W. Field, *Perturbations in the spectra of diatomic molecules (Academic Press, New York, 1986)*.
- [21] J.T. Vanderslice, S.G. Tilford and P.G. Wilkinson, *Astrophys. J.* 142 (1965) 84.
- [22] G.H. Herzberg, *Spectra of diatomic molecules (Van Nostrand, Princeton, 1950)*.
- [23] S.N. Dobryakov and Y.S. Lebedev, *Soviet Phys. Dokl.* 13 (1969) 873.
- [24] J. Janin, *Compt. Rend. Acad. Sci. (Paris)* 217 (1943) 392; 223 (1946) 321.
- [25] A. Lofthus, *Can. J. Phys.* 35 (1957) 216.
- [26] A.G. Gaydon, *Proc. Roy. Soc. A* 182 (1944) 286.
- [27] S.G. Tilford and P.G. Wilkinson, *J. Mol. Spectry.* 12 (1964) 231.
- [28] J. Geiger and B. Schroeder, *J. Chem. Phys.* 50 (1969) 7.
- [29] M. Ogawa and Y. Tanaka, *Can. J. Phys.* 40 (1962) 1593.
- [30] G. Joyez, R.I. Hall, J. Reinhardt and J. Mazeau, *J. Electron Spectry.* 2 (1973) 873.
- [31] P. Hammond, G. King, J. Jureta and F.H. Read, *J. Phys. B* 20 (1987) 4255.
- [32] P.K. Carroll and R.S. Mulliken, *J. Chem. Phys.* 43 (1965) 2170.
- [33] J.W. Ledbetter and K. Dressler, *J. Mol. Spectry.* 63 (1976) 370.